5
Gadolinium Doped Cathode $LiMn_{2-x}Gd_xO_4$ (x=0, 0.01, 0.04, 0.05) Cathodes

The chapter is composed of four sections and eight sub-sections. The section 5.1 presents the introduction about the current chapter. The physical characterizations of gadolinium doped $LiMn_2O_4$ (LMO) cathode powders are presented in section 5.2. The section 5.3 is exploring the electrochemical characterizations of assembled cell with fabricated cathodes. The section 5.2 and section 5.3 are further divided in sub-sections. The section 5.2 is divided in five sub-sections namely: - the sub-section 5.2.1 describes the crystal structural and its analysis, the sub-section 5.2.2 presents the surface morphology findings, the sub-section 5.2.3 gives stoichiometric information, the sub-section 5.2.4 describes thermo-gravimetric performance and in the sub-section 5.2.5 expresses the Raman spectra and its findings. The third section of chapter is also sorted in four sub-sections which include cyclic voltammetry study in the sub-section 5.3.1, galvanostatic charge-discharge performance in the sub-section 5.3.2, rate performance and cyclability analysis in the sub-section 5.3.3 and electrochemical impedance spectroscopy in the sub-section 5.3.4. The concluding remarks are covered in the section 5.4.

5.1 INTRODUCTION

The spinel cathode LMO based lithium ion batteries are particular interest due to its beneficial concerns, abundance and cheap raw material availability, low toxicity, over layered cathode $LiCoO_2$ (LCO) and other similar cathode materials. However, the cathode LMO material is facing major challenge such as capacity fading over long cyclability which imposes limitation on commercial use of it. This issue has multifactor contribution namely-(1) continual Mn dissolution into electrolyte during cycling [Jang et al, 1998; Aoshima et al, 2001], (2) Jahn-Teller distortion [Yamada at el, 1999] and (3) decomposition of electrolyte solution [Gao et al, 1996]. To overcome these challenges, the various strategies are adopted by scientific community and described in detail in Chapter 2 and in section 3.1 of Chapter 3.

The different rare-earth (RE) element doped spinel LMO cathodes have studied in previous Chapter 3 to find out the batter cathode characteristics. It is concluded that gadolinium (Gd) and dysprosium (Dy) doped cathodes are delivered higher specific discharge capacity and increased capacity retention compared to pristine LMO cathode and other rare-earth doped cathodes. To optimize the doping amount of gadolinium (Gd) and dysprosium (Dy), the study is further explored. The current chapter investigates the effect of Gd doping amount. The Gd doping amount is consider ≤2.5% with Mn molar ratio to optimize in the spinel LMO cathode.

For this purpose, the LMO and its gadolinium doped derivatives $LiMn_{2-x}Gd_xO_4$ (x=0, 0.01, 0.04 and 0.05) are synthesized via organic sol-gel method as discussed in sub-section 3.2.2. The surface morphology and structural parameters are studied to investigate the effect of doping amount. The electrochemical characteristics of fabricated cathode are investigated. The cathodes code names are used in further discussion as mentioned in Table 2.1 in Chapter 2. The cathodes full nomenclature may be used to give instant insight whenever it seems to highlight its outcome.

5.2 PHYSICAL CHARACTERIZATION OF GADOLINIUM DOPED $LiMn_{2-x}Gd_xO_4$ CATHODES

The physical characterizations of un-doped LMO and gadolinium doped synthesized powder are carried out by adopting diverse characterization techniques to obtain physical information. These characterization techniques and their analysis are presented in subsequent sub-sections from 5.2.1 to 5.2.5 in sequential way as following:

(5.2.1) *X-ray diffraction and structural analysis* - It presents information about phase formation and lattice parameters.

(5.2.2) *Surface morphology and its analysis* - It offers the powder's surface morphology, geometrical shape and size and the inter planner distance.

(5.2.3) *Energy dispersive X-ray spectra (EDX) and its analysis* – It provides insight about the elemental presence and elemental stoichiometric ratio.

(5.2.4) *Thermo-gravimetric analysis* – It conveys about the thermal stability of synthesized cathode powders are up-to 800 ˚C. The temperature v/s weight loss (%) is also plotted.

(5.2.5) *Raman spectra and its analysis* – It provides the bond strength information about the Mn-O and Gd-O.

5.2.1 X-ray Diffraction and Structural Analysis

The as synthesized powder samples of pristine LMO and its Dy doped derivatives, $LiMn_{2-x}Gd_xO_4$ (x=0.01, 0.04 and 0.05), cathode materials are evaluated for phase formation and their purity. The Figure 5.1 is presenting the powder x-ray diffraction patterns as recorded in red color and its Rietveld fitting in black color. The x-ray diffraction patterns are recorded with scan speed 0.02˚ per second throughout the scanning range 10 - 80 ˚. The more details about the principle and recording parameters of x-ray diffraction are discussed in sub-section 3.3.1 of Chapter 3. The observed diffraction patterns, as in Figure 5.1, are showing the evidence for cubic spinel phase formation in synthesized powders. The peaks are indexing as observed at two theta angle 18.70˚, 36.17˚,37.88˚, 43.97˚, 48.10˚, 58.22˚, 63.96˚, 67.30˚, 75.62˚ and 76.65˚ are assigned to (hkl) planes of lattice structure (111), (311), (222), (400), (331), (511), (440), (531) and very small (553) and (622) respectively. These peaks are similar to phase (JCPDS: 35–782) with the Fd3m space group[Hung et al, 2007]. The Rietveld fitting analysis is also providing good match fitting curves. The additional phases in synthesized powders are also detected. These are correspond to additional phase of $GdMn_2O_5$ and Mn_2O_3 which may be attributed to uncontrolled partial pressure of oxygen during calcinations process [Han et al, 2012; Lee et al, 2014]. The percentage of spinel cubic phase in undoped LMO, LMO-Gd01, LMO-Gd04 and LMO-Gd05 are calculated as 100 %, 58.5 %, 81.53 %, and 82.91 %, respectively. The percentage of additional phases is detected as Mn_3O_4-h (35.78 %), Mn_3O_4-b (2.26 %) and $GdMn_2O_5$ (3.37 %) in LMO-Gd01, $GdMn_2O_5$ (18.45 %) in LMO-Gd04, and $GdMn_2O_5$ (7.75 %), Mn_2O_3 (9.34 %) in LMO-Gd05.The only one additional phase $GdMn_2O_5$ is detected in LMO-Gd04 which is more phase pure then other doped samples. The particle mean size is determined by using Rietveld analysis.

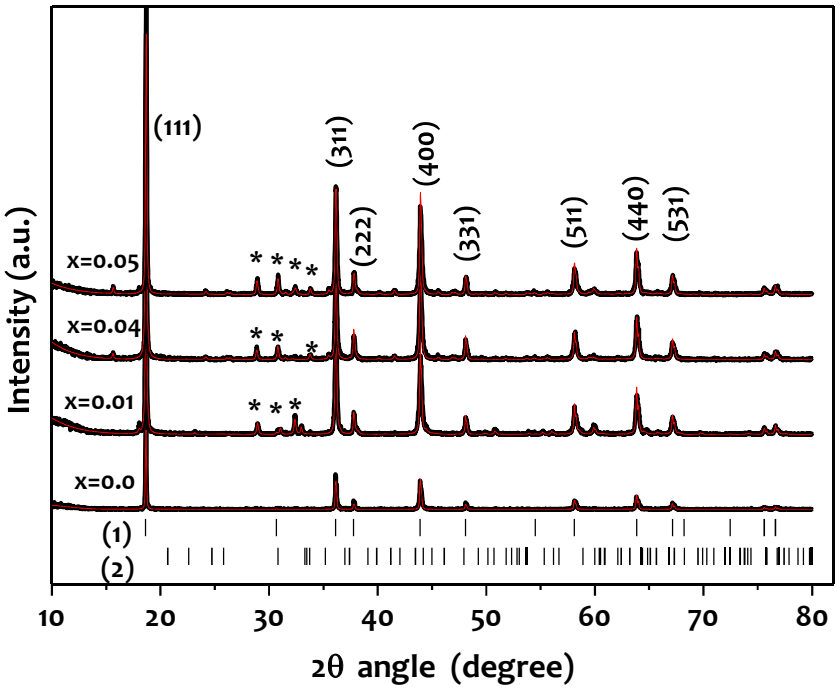

Figure 5.1: Refined (red: calculated; black: experimental) XRD pattern (a) $LiMn_2O_4$, (b) $LiMn_{1.99}Gd_{0.01}O_4$, (c) $LiMn_{1.96}Gd_{0.04}O_4$, and (d) $LiMn_{1.95}Gd_{0.05}O_4$ powders calcined at 800 ˚C / 14 h

The octahedral site occupancy of $Mn^{3+/4+}/Gd^{3+}$ are being calculated using the integral ratio of peaks corresponds to plane (311) to (400) [Ohzuku et al, 2001]. The integral peaks ratio for LMO, LMO-Gd01, LMO-Gd04 and LMO-Gd05 is 1.06, 0.821, 1.151, and 1.025, respectively. It is indicated that Gd has became successful to replace Mn^{3+} ion instead of Mn^{4+} ion in LMO-Gd04 sample compared to other samples. The lattice parameters, unit cell volume, FWHM, crystalline size and integral plane peaks ($I_{(400)}$ /$I_{(311)}$) ratio and impurity in cubic spinel phase are tabulated in Table 5.1.

Table 5.1: Lattice Structure Parameters of $LiMn_2O_4$ and $LiMn_{2-x}Gd_xO_4$ (x = 0, 0.01, 0.04, 0.05) Powders

Sample Description	*Lattice Parameters*	*Unit cell Volume*	*FWHM*	*Crystallite Size*	*Rietveld Phase Purity*	$I_{(400)}/I_{(311)}$
	(Å)	(Å³)	(°)	(Å)	(%)	
LMO	8.240	559.500	0.104	518.16	100	1.096
LMO-Gd01	8.239	559.233	0.130	620.76	58.5	0.821
LMO-Gd04	8.233	558.824	0.139	664.78	81.53	1.151
LMO-Gd05	8.231	557.721	0.131	625.60	82.91	1.025

5.2.2 Surface Morphology Study and Its Analysis

The surface information of synthesized active cathode materials, $LiMn_{2-x}Gd_xO_4$ (x=0, 0.01, 0.04 and 0.05) are recorded using scanning electron microscopy (SEM) and shown in Figure 5.2. The surface morphology has polyhedral geometry with irregular shape and size. The smaller granules are agglomerated to form larger particles which are evidenced by the presence of smaller grains. The agglomeration is straightforward. This means that the material has tendency to agglomerate. The particle size is varied from micrometer range to nano-range. However, the Gd doped cathodes have more uniformity and less agglomerate tendency

compared to un-doped LMO cathode powder as can be seen through pictorial view in Figure 5.2 (a, c and f). The similar tendency is observed for the sample LMO-Gd05.

To inspect the nano-scopic view of surface morphology and inter-planner distance the high resolution tunneling electron microscopy (HRTEM) are carried out. The HRTEM images of LMO, LMO-Gd01 and LMO-Gd04 are shown in Figure 5.2 (b, d, and f). The inter-planner distance is found 0.42 nm in the case of LMO-Gd04 which seem to be increased in comparison to LMO (0.23 nm) and LMO-Gd01 (0.25 nm). It is direct evidence that size of lattice is increased after Gd doping.

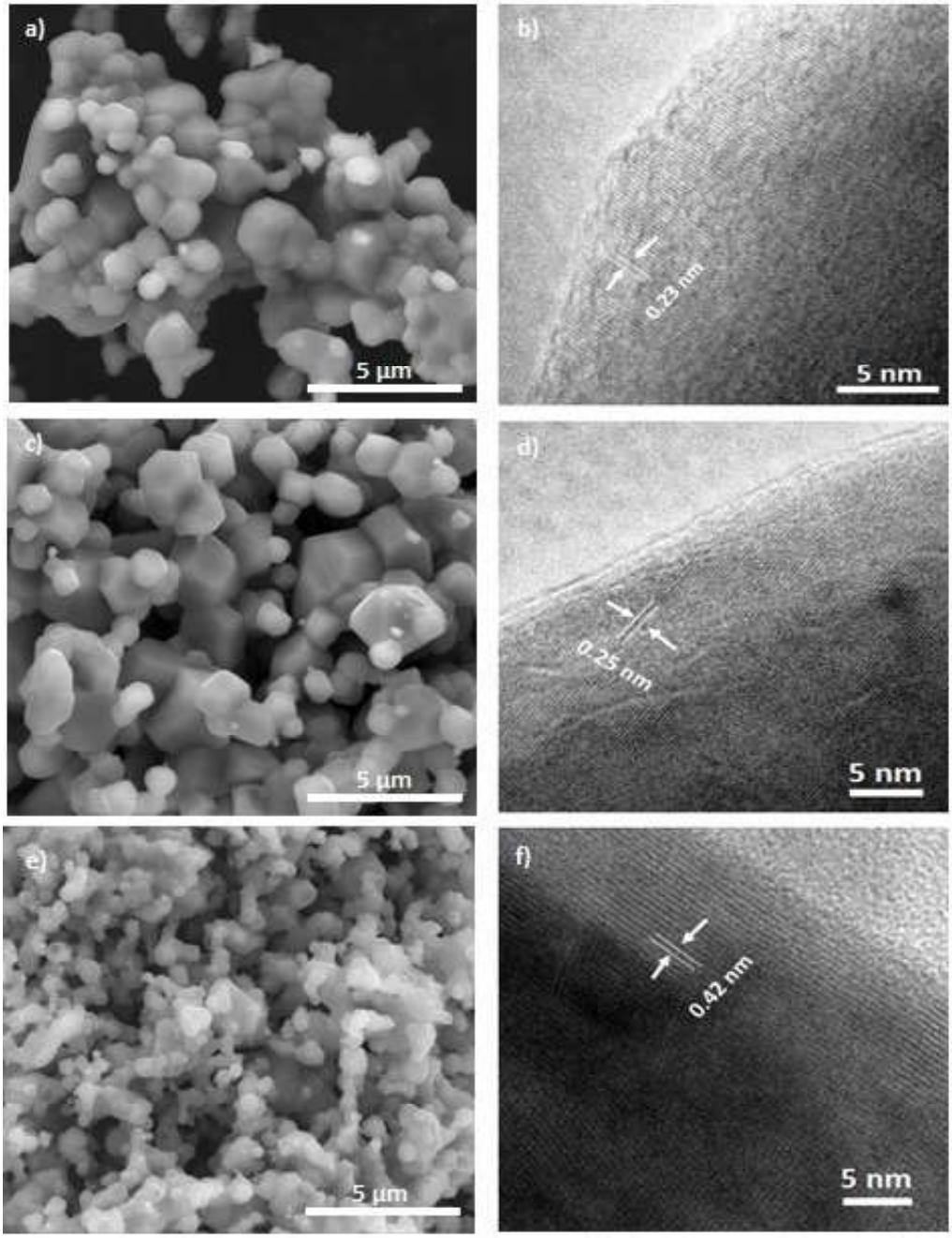

Figure 5.2: SEM (a, c and e) and HRTEM (b, d and f) images of the synthesized $LiMn_{2-x}Gd_xO_4$ powders with x=0 (a, b), x=0.01 (c, d) and x=0.04 (e, f)

5.2.3 Energy Dispersive X-ray Spectra (EDX) and Its Analysis

The presence of elements in synthesized powders is detected by using the attached EDX accessory, Oxford instruments, with SEM (Brucker EVO special edition). The powder materials are in pure elemental form due to absence of other elements in synthesized matrices. The atomic and weight percentage are tabulated in Table 5.2. The theoretical atomic percentage of Mn and O in LMO are 33.33% and 66.66% respectively. However, the accuracy is less in detection of O element using EDX assembly attached with SEM [SEM]. The 0.83% and 32.5% atomic percentage of Gd and Mn elements are received in LMO-Gd05 cathode powder. The measured elemental percentage is nearby equal as desired theoretical. The representative the spectrum as recorded from EDX assembly attached with SEM is presented in Figure 5.3

Table 5.2: Elemental Composition in $LiMn_{2-x}Gd_xO_4$ (x=0, 0.01, 0.04 and 0.05) Powders

Sample Description	*Observed Atomic (%)*			*Theoretical Atomic (%)*		
	Mn	*O*	*Gd*	*Mn*	*O*	*RE*
LMO	33.44	66.56	0.0	33.33	66.66	0.0
LMO-Gd01	31.33	68.43	0.23	33.17	66.66	0.17
LMO-Gd04	33.57	65.69	0.84	32.67	66.66	0.67
LMO-Gd05	38.53	60.56	0.91	32.5	66.66	0.83

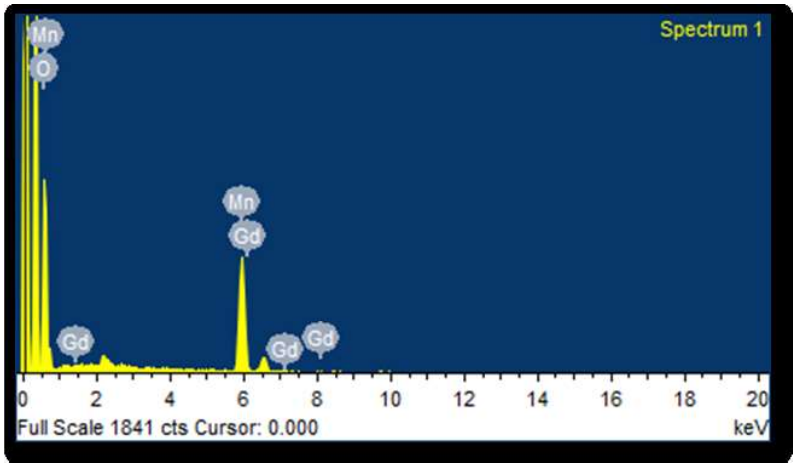

Figure 5.3: EDX elemental spectrum of $LiMn_{2-x}Gd_xO_4$ (x=0, 0.01, 0.04 and 0.05) powders calcined at 800 ˚C / 14 h

5.2.4 Thermal-Gravimetry and Its Analysis (TGA)

To ensure the crystal structure stability of as synthesized active cathode derivatives; $LiMn_{2-x}Gd_xO_4$ (x=0, 0.01, 0.04 and 0.05); the thermo-gravimetric data are recorded with heating rate 10 ˚C per minute after calcined samples. The weight-loss (%) is recorded with temperature from room temperature (~ 30 ˚C) to high temperature 800 ˚C. The recorded spectra are shown in Figure 5.4.

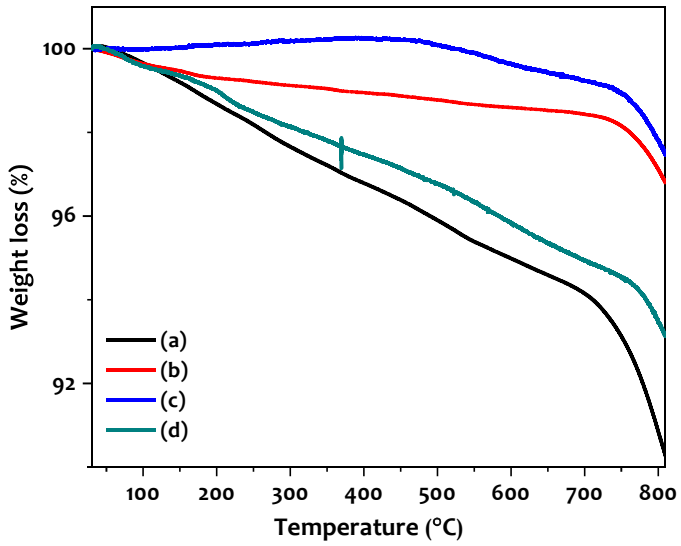

Figure 5.4: Thermal-gravimetric graphics of (a) $LiMn_2O_4$, (b) $LiMn_{1.99}Gd_{0.01}O_4$, (c) $LiMn_{1.96}Gd_{0.04}O_4$, and (d) $LiMn_{1.95}Gd_{0.05}O_4$, powder calcined at 800 ˚C / 14 h

The thermal stability of as synthesized cathode materials is stable to extent. The low weight-loss is observed up-to 700 ˚C. It is indicating stable phase formation is taking place. As amount of Gd is increased, the thermal stability of $LiMn_2O_4$ crystalline structure is also improved. However, the LMO-Gd05 is showing less stable compared to LMO-Gd01 and LMO-Gd04.

The weight-loss are observed less than 0.5% for LMO and LMO-Gd01 and even less for LMO-Gd04 and LMO-Gd05 at around 100 ˚C. It may be attributed to water moisture released during heating process. Above 100 ˚C on wards the continual low weight loss observed in all samples. It is supported to stable phase formation and low exchange of O atom exchange behavior in stable phase at high temperature. However, in the case of LMO the weight loss is more compared to Gd doped cathodes. It is revealed that more O-atoms exchange take place which degrade structure stability of active cathode material. When temperature increases beyond 700 ^{O}C, the rapid weight-loss is appeared in all cathodes. It is due to loss of oxygen or new phase formation, as $Li_2Mn_2O_4$, is taking place [Dziembaj and Molenda, 2003].

5.2.5 Raman Spectrum and Its Analysis

The Figure 5.5 shows the Raman spectra of as synthesized LMO and gadolinium doped derivatives ($LiMn_{2-x}Gd_xO_4$; x= 0.0, 0.01, and 0.04). Raman spectrum of LMO-Gd05 is performed due to poor spinel structure and appearance of more additional. There are one strong peak at 620 cm^{-1} and one weak shoulder at 590 cm^{-1} are observed in all spectra. The intense peak at 620 cm^{-1} corresponds to Mn-O symmetric vibration mode [Ramana et al, 2005; Liu et al, 2012]. The symmetric vibration in the MnO_6 group is due to A_{1g} symmetry in the O^7 h space group [Prabaharan et al, 1998]. As Gd elemental content is increased the broadening in peak corresponds to 620 cm^{-1} is also increased. The broadening is corresponds to the increment in lattice structure between the isotropic $Mn^{4+}O_6$ octahedral and local distorted $Mn^{3+}O_6$ octahedral in LMO [Liu et al, 2012]. The weak shoulder at 590 cm^{-1} may be assigned to symmetric bending vibration mode (F_{2g}) of Mn-O bond [Julien and Massot, 2003]. It is clear shown that low amount of Gd doping has negligible effect on vibration modes of LMO cathode. The vibration energy of these modes depends upon the concentration of Mn^{4+}-ion in the active material and reflects the Mn average oxidation state [Liu et al, 2012].

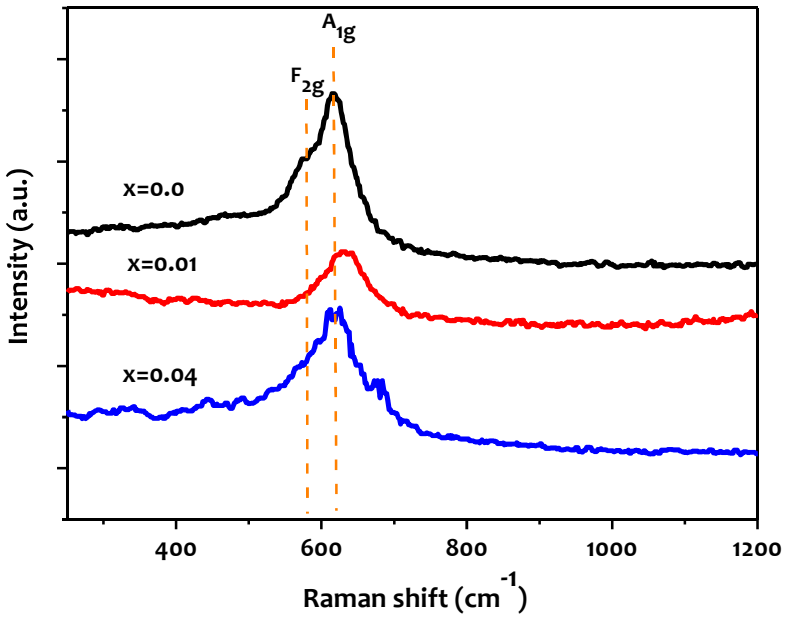

Figure 5.5: Raman spectra of (a) $LiMn_2O_4$, (b) $LiMn_{1.99}Gd_{0.01}O_4$ and (c) $LiMn_{1.96}Gd_{0.04}O_4$, powder calcined at 800 °C / 14 h

5.3 ELECTROCHEMICAL CHARACTERIZATION OF GADOLINIUM DOPED $LiMn_{2-x}Gd_xO_4$ CATHODES

Once physical characterizations of synthesized cathode material, $LiMn_{2-x}Gd_xO_4$ (x=0, 0.01, 0.04 and 0.05), are finished. Then, it becomes essential to analyze the battery performance of these cathode materials. The as synthesized un-doped and Gd doped cubic spinel phase cathode powders are characterized electrochemically to evaluate the influence of doping amount. The electrochemical performances of active material are assessed by using cyclic voltammetry technique, galvano-static charge-discharge technique, and AC impedance spectroscopy technique. The details about these characterization techniques are presented in section 3.4 of Chapter 3 and analysis sections are presented in following sub-sections from 5.3.1 to 5.3.4. The characteristics are performed on two/three electrode Swagelok cell assembly. The assembling of the Swagelok cell is given in sub-section 3.4.1.4 of Chapter 3.

(5.3.1) *Cyclic Voltammetry Technique* is exploring the redox potentials of cathode materials

(5.3.2) *Galvanostatic Charge-discharge technique* is using to assess the specific charge-discharge capacity at different charging and discharging rates i.e. C-rate.

(5.3.3) *Rate performance and cyclability measurement* are measuring the capacity fading, columbic efficiency at different C-rates. It also describes the charge-discharge cyclic study up-to 50 cycles at C/2 rate.

(5.3.4) E*lectrochemical impedance spectroscopy* is assessing the internal impedance of fabricated cell is assessed. The internal AC impedance is measured by applying 10mV ac voltage signal over open circuit potential (OCP).

5.3.1 Cyclic Voltammetry and Its Analysis

The second cycle of cyclic voltammetry performance on three electrodes swagelock cell, $LiMn_{2-x}Gd_xO_4$ (x=0, 0.01, 0.04 and 0.05), are shown in Figure 5.6 for spinel cathode and its derivatives. The two oxidation (4.1/4.2V) and two reduction peaks (3.9/4.1 V) are evidence of two stage Li^+-ion intercalation/de-intercalation process [Zhao et al, 2012]. The oxidation and reduction potential are tabulated in Table 5.3. The intense peak in cathode material LMO-Gd01 in comparison to other cathode LMO and LMO-Gd04 is observed. It shows that the low

impedance and easy Li-ion diffusion take place in the LMO-Gd01 cathode. The oxidation and reduction potential are shifted toward the lower potential which indicates the lower polarization potential in the LMO cathode. It may be attributed to other phases support. The lower values of ΔE_c in all the Gd doped cathode samples are indicating reduction in electrode polarization which is a result of small particle size. The cathode LMO-Gd01 is showing the equal values of ΔE_c and ΔE_a. This confirms that there is no polarization effect during charging and discharging [IIango et al, 2015]. The reduced polarization effect is also observed in LMO-Gd04 and LMO-Gd05 cathodes.

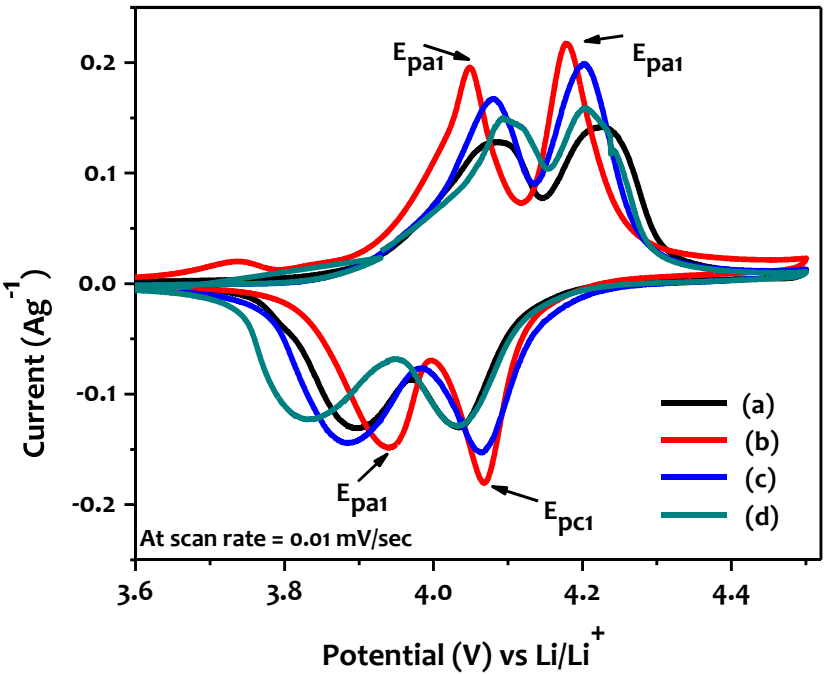

Figure 5.6: Cyclic voltammetry of (a) $LiMn_2O_4$, (b) $LiMn_{1.99}Gd_{0.01}O_4$, (c) $LiMn_{1.96}Gd_{0.04}O_4$, and (d) $LiMn_{1.95}Gd_{0.05}O_4$ cathodes

Table 5.3: Redox Potential of $LiMn_2O_4$ and $LiMn_{2-x}Gd_xO_4$ (x = 0.01, 0.04 and 0.05) Cathodes

Sample Description	*Potential (V)*					
	E_{pa1}	E_{pa2}	E_{pc1}	E_{pc2}	ΔE_{p1}	ΔE_{p2}
$LiMn_2O_4$	4.09	4.23	3.89	4.03	0.20	0.20
$LiMn_{1.99}Gd_{0.01}O_4$	4.05	4.18	3.94	4.07	0.11	0.11
$LiMn_{1.96}Gd_{0.04}O_4$	4.08	4.20	3.88	4.06	0.20	0.14
$LiMn_{1.95}Gd_{0.05}O_4$	4.10	4.21	3.82	4.03	0.28	0.18

5.3.2 Galvanostatic Charge-Discharge Performance

The galvanostatic charge-discharge capacity of assembled two electrode Swagelok cells is carried out at different C-rates; C/10, C/5, C/2, 1C and C/10 (recv.); and up-to different cycles. The C-rate calculation, charge-discharge program, cyclability are already discussed in sub-section 3.3.3 and 3.3.4 of Chapter 3. All tests are performed at room temperature. The charge-discharge curves are having two plateaus which reveal that Li+ ion intercalation/de-intercalation is occurring in two stages.

The initial specific charge capacities are 146.3, 116.0, 124.9, 111.9 $mAhg^{-1}$ for LMO, LMO-Gd01, LMO-Gd04, and LMO-Gd05, respectively whereas initial specific discharge capacities are observed 93.5, 106.3, 115.9, and 85.3 $mAhg^{-1}$ for LMO, LMO-Gd01, LMO-Gd04, and LMO-Gd05, respectively at C/10 rate. The specific charge-discharge capacity is observed high for the

$LiMn_{1.96}Gd_{0.04}O_4$ cathode. The specific charge-discharge capacity curves are presented in Figure 5.7 (a-b) for LMO-Gd04 cathode. The specific charge-discharge performance up-to initial five cycles at C/10 rate are shown in Figure 5.7 (a) whereas the specific discharge capacities at C/10, C/5, C/2, C, and C/10(rec.) rate for after 5th cycle are shown in Figure 5.7 (b). The capacity retention after 5 cycles is 91.55%, 68.57%, 96.38%, and 78.66% for LMO, LMO-Gd01, LMO-Gd04, and LMO-Gd05, respectively. It is concluded that synthesized LMO-Gd04 cathode is delivering improved capacity and capacity retention among other cathodes. The discharge capacities at higher C- rates, C/5, C/2, C and recovery cycle at C/10 for LMO-Gd04 cathode are measured as 111.7, 89.6, 76.2, 47.4 and 96.9 $mAhg^{-1}$ after 5th cycle at each C-rate. These discharge capacities are improved over the other Gd doped derivatives and pristine lithium manganese oxide spinel cathode.

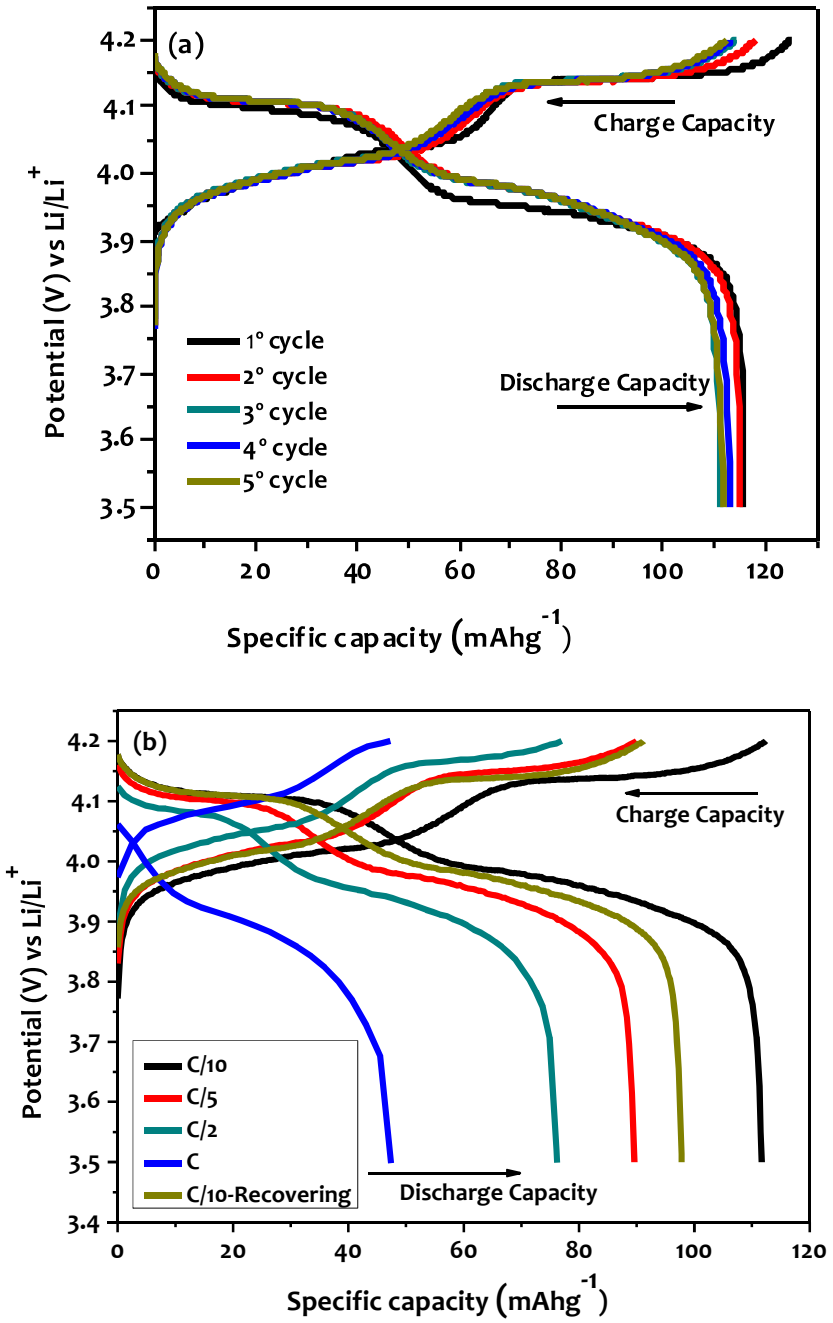

Figure 5.7: Charge-discharge capacity curve of $LiMn_{1.96}Gd_{0.04}O_4$ cathode (a) Initial to 5th cycles at C/10 rate and (b) C/10 to C for the 5th cycle

The comparison of discharge capacities of LMO and $LiMn_{2-x}Gd_xO_4$ (x = 0.01, 0.04 and 0.05) spinel cathodes at C/10 and at C rate are shown in Figure 5.8. The capacity retention after 5th cycles at C/10 rate is measured as 85.6, 72.9, 111.7 and 67.1 $mAhg^{-1}$ for LMO and $LiMn_{2-x}Gd_xO_4$ (X = 0.01, 0.04 and 0.05) respectively as shown in Figure 5.8 (a) and tabulated in Table 5.4. At 1C, the capacity retention after 5th cycles is observed as 31.7, 4.9, 47.4 and 26.4 $mAhg^{-1}$ for LMO and $LiMn_{2-x}Gd_xO_4$ (x = 0.01, 0.04 and 0.05), respectively, as shown in Figure 5.8 (b) and Tabulated in 5.8. The study is revealing that cathode LMO is showing improved discharge capacity at each C-rate compared to pristine and other Gd doped cathodes. The poor performance of LMO-Gd01, Figure 5.8 (a & b), is attributed to lower phase purity as evidenced in x-ray diffraction study.

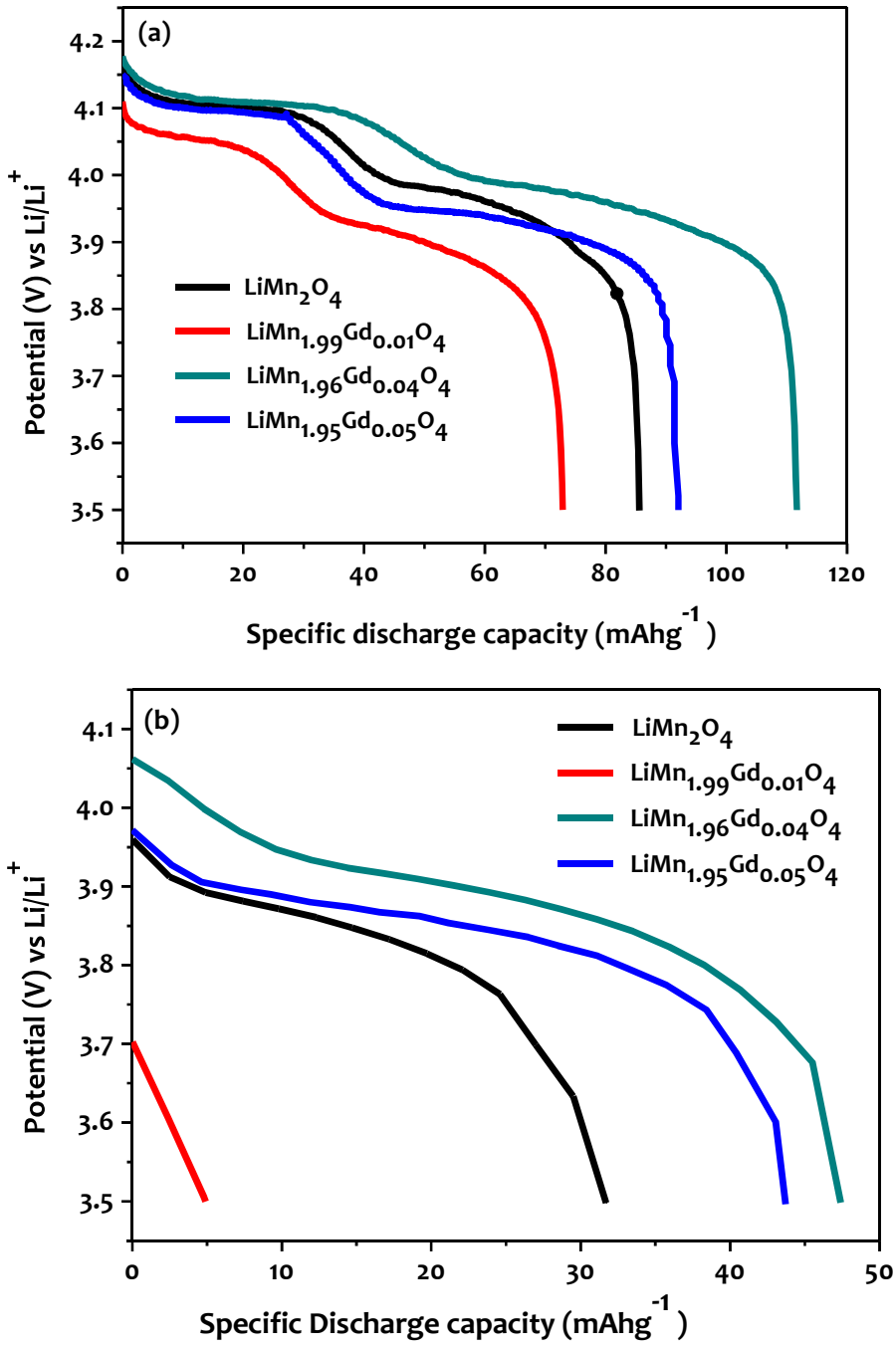

Figure 5.8: Comparison of discharge capacity for all cathodes: (a) at C10 and (b) C for the 5th cycle

Table 5.4: Charge-Discharge Capacities of $LiMn_2O_4$ and $LiMn_{2-x}Gd_xO_4$ (x = 0.01, 0.04 and 0.05) Cathodes at C/10 Rate

Sample Description	*Charging Capacity ($mAhg^{-1}$)*	*Discharging Capacity ($mAhg^{-1}$)*	*Charging Capacity ($mAhg^{-1}$)*	*Discharging Capacity ($mAhg^{-1}$)*	*Discharge Capacity Fading*	*Columbic Efficiency*
	At 1^{st} cycle	At 1^{st} cycle	At 5^{th} cycle	At 5^{th} cycle	After 5^{th} cycle (%)	I^{st} cycle (%)
$LiMn_2O_4$	146.3	93.5	87.5	85.6	8.45	63.91
$LiMn_{1.99}Gd_{0.01}O_4$	116	106.3	78.6	72.9	31.43	91.63
$LiMn_{1.96}Gd_{0.04}O_4$	124.9	115.9	112.4	111.7	3.62	92.79
$LiMn_{1.95}Gd_{0.05}O_4$	120.1	113.2	99.9	91.1	19.52	94.25

Table 5.5: Charge-Discharge Capacities of $LiMn_2O_4$ and $LiMn_{2-x}Gd_xO_4$ (x = 0.01, 0.04 and 0.05) Cathodes at C/5 Rate

Sample Description	*Charging Capacity ($mAhg^{-1}$)*	*Discharging Capacity ($mAhg^{-1}$)*	*Charging Capacity ($mAhg^{-1}$)*	*Discharging Capacity ($mAhg^{-1}$)*	*Discharge Capacity Fading*	*Columbic Efficiency*
	At 1^{st} cycle	At 1^{st} cycle	At 5^{th} cycle	At 5^{th} cycle	After 5^{th} cycle (%)	I^{st} cycle (%)
$LiMn_2O_4$	82.8	79.8	74.6	73.4	8.02	96.38
$LiMn_{1.99}Gd_{0.01}O_4$	77.2	72.5	66.4	64.7	11.45	93.91
$LiMn_{1.96}Gd_{0.04}O_4$	98.8	93.9	90	89.6	4.58	95.04
$LiMn_{1.95}Gd_{0.05}O_4$	100.7	98.5	97.9	94.5	4.06	97.82

Table 5.6: Charge-Discharge Capacities of $LiMn_2O_4$ and $LiMn_{2-x}Gd_xO_4$ (x = 0.01, 0.04 and 0.05) Cathodes at C/2 Rate

Sample Description	*Charging Capacity ($mAhg^{-1}$)*	*Discharging Capacity ($mAhg^{-1}$)*	*Charging Capacity ($mAhg^{-1}$)*	*Discharging Capacity ($mAhg^{-1}$)*	*Discharge Capacity Fading*	*Columbic Efficiency*
	At 1^{st} cycle	At 1^{st} cycle	At 5^{th} cycle	At 5^{th} cycle	After 5^{th} cycle (%)	I^{st} cycle (%)
$LiMn_2O_4$	65.1	61.8	58	57.5	6.96	94.93
$LiMn_{1.99}Gd_{0.01}O_4$	43.9	40.8	41	40.6	0.04	92.94
$LiMn_{1.96}Gd_{0.04}O_4$	80.2	75.8	77.0	76.2	+0.05	94.51
$LiMn_{1.95}Gd_{0.05}O_4$	79.9	75.7	76.3	76.1	-0.53	94.74

Table 5.7: Charge-Discharge Capacities of $LiMn_2O_4$ and $LiMn_{2-x}Gd_xO_4$ (x = 0.01, 0.04 and 0.05) Cathodes at C Rate

Sample Description	*Charging Capacity ($mAhg^{-1}$)*	*Discharging Capacity ($mAhg^{-1}$)*	*Charging Capacity ($mAhg^{-1}$)*	*Discharging Capacity ($mAhg^{-1}$)*	*Discharge Capacity Fading*	*Columbic Efficiency*
	At 1^{st} cycle	At 1^{st} cycle	At 5^{th} cycle	At 5^{th} cycle	After 5^{th} cycle (%)	I^{st} cycle (%)
$LiMn_2O_4$	33.8	32.2	31.7	31.7	1.55	95.27
$LiMn_{1.99}Gd_{0.01}O_4$	6.4	5.2	4.6	4.9	0.06	96.67
$LiMn_{1.96}Gd_{0.04}O_4$	52.7	50.5	47.3	47.4	6.1	94.93
$LiMn_{1.95}Gd_{0.05}O_4$	45.0	43.5	43.8	43.8	-0.69	96.67

5.3.3 Rate Performance and Cyclability Analysis

The discharge rate performance at different C-rate of different cathodes is presented in Figure 5.9 (a) whereas the cyclability and columbic efficiency up-to 40 cycles at C/2 rate for LMO and LMO-Gd04 are presented in Figure 5.9 (b). The cathode LMO-Gd04 is showing improved discharge capacity at each C-rate. The specific discharge capacity for LMO and LMO-Gd04 at C/2 are obtained as 47.0, 70.3 and 33.2, 59.5 $mAhg^{-1}$ at the 1st and the 40th cycle, respectively. The decrement in capacity after 40th cycle for LMO and LMO-Gd04 is recorded as 14 and 13.7 $mAhg^{-1}$, respectively. It is revealed that LMO-Gd04 spinel cathode has less capacity fading compared to un-doped LMO. The columbic efficiency in the both cathodes is achieved near to 100% after each cycle [Ram et al, 2017].

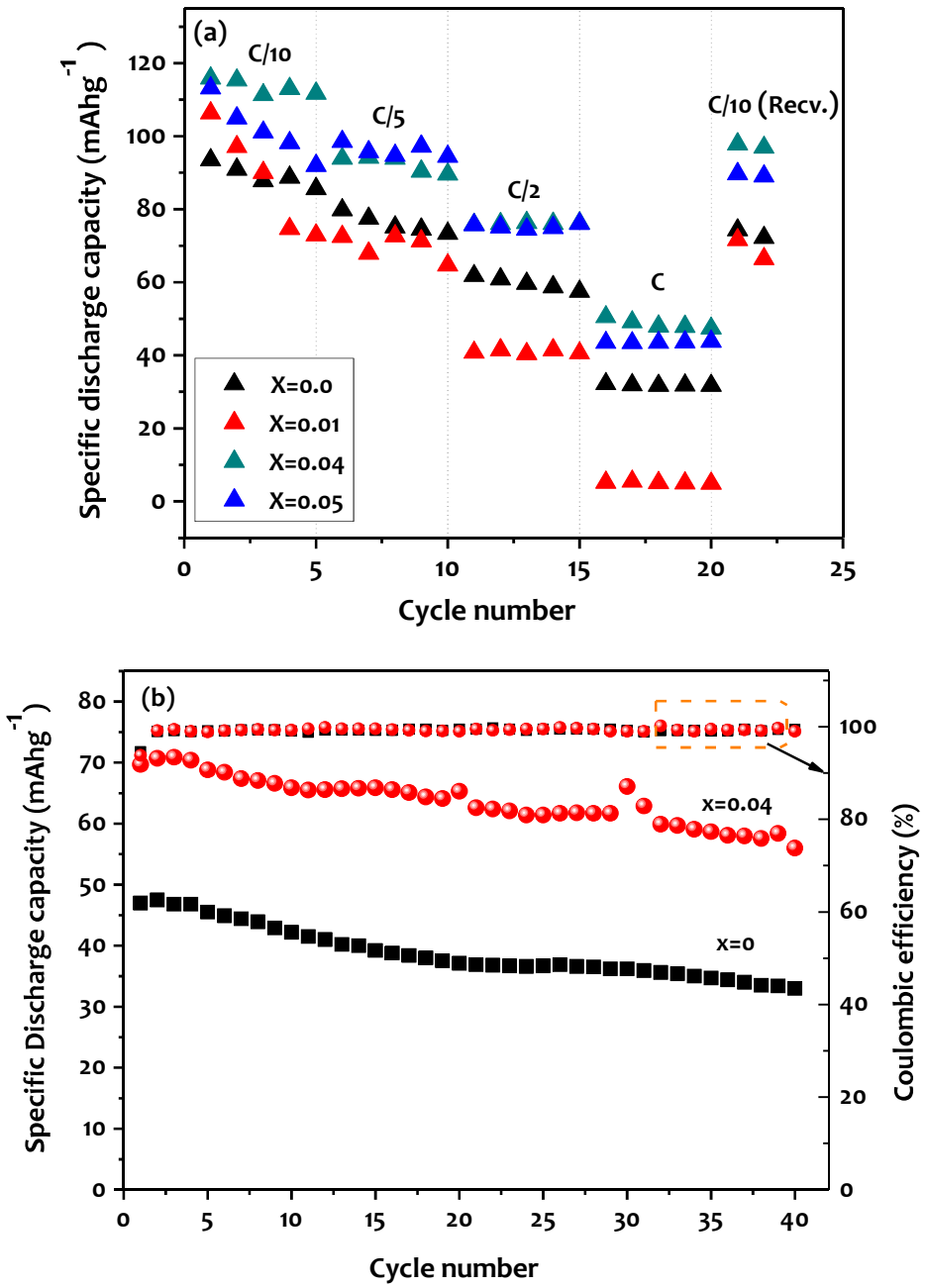

Figure 5.9: For $LiMn_{2-x}Gd_xO_4$ (x=0, 0.01, 0.04 and 0.05) (a) specific discharging rate performance up to 5th cycle at different C-rates and (b) Cyclability up to 40 cycles at C/2 rate and columbic efficiency

Table 5.8: Charge-Discharge Capacities of $LiMn_2O_4$ and $LiMn_{2-x}Gd_xO_4$ (x = 0.01, 0.04 and 0.05) Cathodes at C/10 (Recv.) Rate

Sample Description	*Charging Capacity ($mAhg^{-1}$)*	*Discharging Capacity ($mAhg^{-1}$)*	*Charging Capacity ($mAhg^{-1}$)*	*Discharging Capacity ($mAhg^{-1}$)*	*Discharge Capacity Fading*	*Columbic Efficiency*
	At 1st cycle	At 1st cycle	At 2nd cycle	At 2nd cycle	After 2nd cycle (%)	Ist cycle (%)
$LiMn_2O_4$	69.8	74.3	74.6	72.2	2.83	106.45
$LiMn_{1.99}Gd_{0.01}O_4$	69.5	71.6	68.4	66.4	7.26	103.02
$LiMn_{1.96}Gd_{0.04}O_4$	91.2	97.8	96.9	96.9	0.09	107.23
$LiMn_{1.95}Gd_{0.05}O_4$	74.3	77.1	80.8	72.8	5.58	103.77

5.3.4 Electrochemical Impedance Spectroscopy

To investigate the effect of varied amount Gd doping on over all internal impedance of cathode materials, the three electrode Swagelok cell is fabricated. The AC impedance spectroscopy is used to measure the internal impedance. The 10 mV amplitude (peak to peak) ac signal over the open circuit potential is applied after 2nd cycle of cylic voltammetry. The AC signal frequency is scanned from 10^{+6} Hz to 10^{-3}Hz from higher to lower frequency. The Nyquist plots, as shown in Figure 5.10, are drawn to analyze the impedance behavior of assembled three electrode cell. The LMO cathode is showing depressed semi circle in middle frequency range and bit steep increasing in higher frequency range. The LMO-Gd01 cathode is showing the two depressed semi-circle and lower and middle frequency region with steep slope at higher frequency region. The LMO-Gd04 cathode is representing large and clear semi-circle at middle frequency region and low slop at high frequency region. It is evident that LMO-Gd04 offer more impedance compare to other spinel cathodes [Ram et al, 2017]

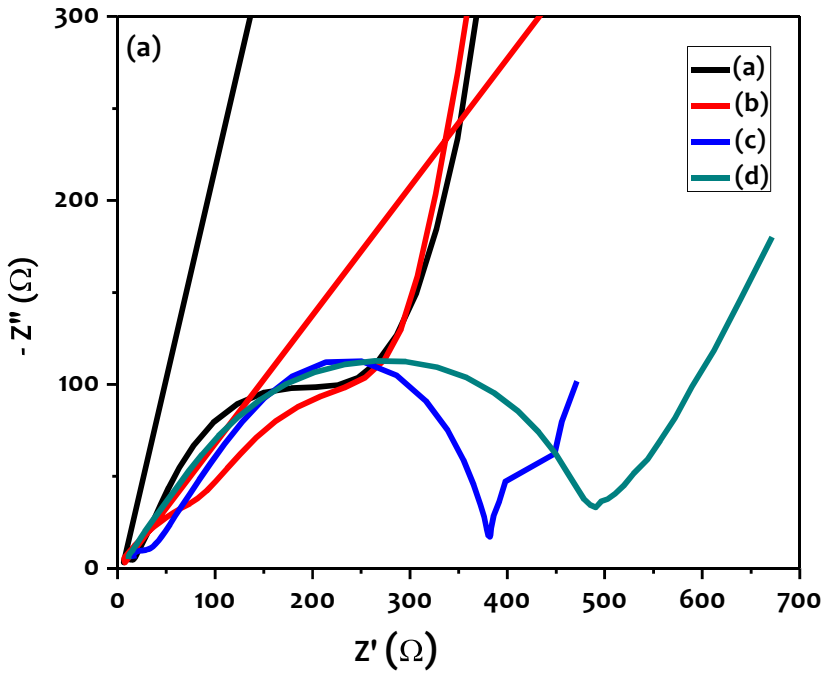

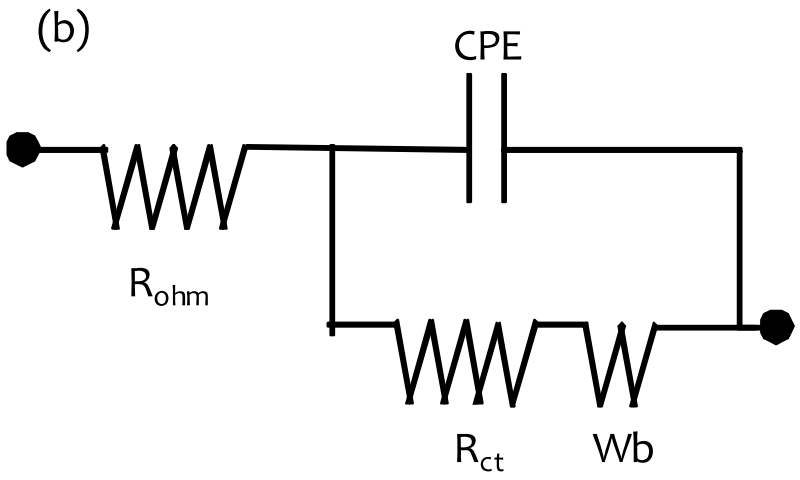

Figure 5.10: EIS spectra of (a) $LiMn_2O_4$ (b) $LiMn_{1.99}Gd_{0.01}O_4$, (c) $LiMn_{1.96}Gd_{0.04}O_4$, and (d) $LiMn_{1.95}Gd_{0.05}O_4$ cathodes, (b) Its representative electrical circuit

5.4 CLOSING REMARKS

The low amount gadolinium (Gd) rare earth elemental doped spinel cathode, $LiMn_{2-x}Gd_xO_4$ (x = 0.0, 0.01, 0.04 and 0.05), are synthesized successfully by adopting organic sol-gel method.

The initial discharge capacities for LMO, LMO-Gd01, LMO-Gd04 and LMO-Gd05 are 93.5, 106.3, 115.9, 85.3; 79.8, 72.5, 93.9, 61.0; 61.8, 40.8, 75.8, 45.9; 32.2, 4.6, 47.3, 26.3 and 74.3, 71.6, 97.8, 82.8 mAh^{-1} at C/10, C/5, C/2, 1C and C/10 (recv.) respectively. The capacity retention after 40 cycles is observed as 70.64% and 84.63% for LMO and LMO-Gd04, respectively.